Supplementary Materials for

Gradient matters via filament diameter-adjustable 3D printing

Huawei Qu[1,2], Chongjian Gao[1], Kaizheng Liu[1], Hongya Fu[2], Zhiyuan Liu[3,4], Paul H. J. Kouwer[5], Zhenyu Han[2*] & Changshun Ruan[1,4*]

[1] Research Center for Human Tissue and Organs Degeneration, Institute of Biomedicine and Biotechnology, Shenzhen Institute of Advanced Technology, Chinese Academy of Sciences, Shenzhen 518055, China.

[2] School of Mechatronics Engineering, Harbin Institute of Technology, Harbin 15000, China.

[3] Research Center for Neural Engineering, Shenzhen Key Laboratory of Smart Sensing and Intelligent Systems, Shenzhen Institute of Advanced Technology, Chinese Academy of Sciences, Shenzhen 518055, China.

[4] University of Chinese Academy of Sciences, Beijing 100049, China.

[5] Institute for Molecules and Materials, Radboud University, Nijmegen 6525 AJ, The Netherlands.

* e-mail: hanzy@hit.edu.cn (Z.H.); cs.ruan@siat.ac.cn (C.R.)

This PDF file includes:

Other Supplementary Materials for this manuscript include the following:

Materials and Methods

Materials

Low Mn polycaprolactone (PCL) (Aldrich, average Mw ~14,000, product No. 440752), high Mn PCL (Aldrich, average Mw 45,000, product No. 704105), β-tri-calcium phosphate (β-TCP) (Sigma-Aldrich, product No. 49963), polyethylene-polypropylene glycol (Polyether F127) (Macklin, average Mn ~13,000, product No. P822479), alginate (Sigma, low viscosity, product No. A1112), calcium chloride anhydrous (Ca^{2+}) (Aldrich, product No. C110766), gelatin from porcine skin (Vetec, product No. V900863), methacrylic anhydride (Aldrich, product No. 276685), photoinitiator 2-hydroxy-2-methyl-1-phenyl-1-propanone (Sigma-Aldrich, Irgacure 1173, product No. 405655), polydimethylsiloxane (PDMS) (Dowsil, SE1700 clear), and liquid metals (LMs) EGaIn (Dingguan metal technology company) were procured and employed for experimentation directly without any modification.

Ink preparation

To prepare L-PCL, low Mn PCL and β-TCP powder with a 4:1 weight-to-weight ratio were heated in a beaker at 60 °C for 30 minutes and then stirred with a glass rod. The above steps were repeated 5 times. Next, the mixed material was extruded through a lab-accessible 3D printer with a nozzle inner diameter of 400 μm after holding at 60 °C for 30 minutes. The preparation process of H-PCL was similar to that of L-PCL ink, except that L-PCL was replaced by H-PCL and the heating temperature was increased to 110 °C. The rheological properties of the two inks, L-PCL and H-PCL, are shown in **Supplementary Figure 3**.

The inks for coaxial printing include core and shell material (**Supplementary Figure 12**). For vascular scaffolds (**Fig. 4c**), the core ink, a sacrificial material, was obtained by mixing F127 and deionized water in a 4:1 weight-to-volume ratio. The shell ink was a mixture of gelatin methacryloyl (GelMA) hydrogel and 1 wt% photoinitiator (Irgacure 1173), where GelMA was obtained from gelatin and methacrylic anhydride according to the reported method[1]. For flexible electronics (**Fig. 4d**), the core material is a liquid metal, and the shell material is PDMS obtained by mixing the substrate and catalyst in a 10:1 weight-to-weight ratio. The F127, GelMA, and PDMS inks were transferred into the barrel, and then centrifuged at 2000 rpm for 5 minutes to remove air bubbles.

For the ink preparation of 4D printing (**Fig. 4e**), a 5:2 weight-to-weight ratio of deionized water and pure alginate was mixed homogeneously at room temperature (25 °C). The obtained mixture was transferred to the barrel, and then centrifuged at 2000 rpm for 5 minutes.

Equation derivation of basic fluid continuity

Given volume conservation, the following three equations can be obtained: (i) the volume ΔV_{ink} of ink extruded from the nozzle at unit time Δt is $\Delta V_{ink} = Q \times \Delta t$; (ii) the volume of deposited filament at unit length Δl is $\Delta V_{ink} = S \times \Delta l$, where $S = \pi D^2/4$ is the cross-sectional area of deposited filament, and D is the ideal filament diameter; and (iii) the length of deposited filament at unit time Δt is $\Delta l = V \times \Delta t$, where V is the printing velocity. The above equations are combined to obtain equation (1).

Design-to-fabrication workflow

A CAD software (Rhinoceros 3D® embedded with a parametric design tool Grasshopper, Robert McNeel & Associates, https://www.rhino3d.com/), a desktop computer (DELL®), a commercially available extrusion 3D printer (Regenovo Bio-Architect® WS, Hangzhou Regenovo Biotechnology), and a control software matching the 3D printer (3D Bio-Architect®) were used to building the design-to-fabrication workflow for the FDA-3DP strategy.

In the design workflow **(Extended Data Figs. 5-6)**, first, the original grid curves (0°/90°) were drawn in the parametric software Grasshopper according to the geometry of the target model, and the results were displayed simultaneously in the working interface of the software Rhino. Second, the number of aliquot points on the grid curves was determined based on the fabrication resolution of 1.25 mm. Third, the filament diameter at each point of the grid curves was determined based on the design gradient of the pore size, whereby constructing a filament-filled 3D model with FDA layers. The fourth is optional, if there was a local collapse in the model, supporting layers with a constant minimum filament diameter D_{min} (relative to the range of FDA layers) were added at the desired location. The printing trajectory of the supporting layer is also the grid curve, which differs in that its length depends on Boolean intersection operations. Notably, it is not that all the FDA layers were stacked and then all supporting layers were deposited layer-by-layer. The deposition of these layers was crossed, and each supporting layer was added to the FDA layers with judgment. If the thickest location of the collapsed area obtained without adding a supporting layer exceeds the minimum diameter, a supporting layer needs to be placed. Finally, the 3D model of gradient pore structures was developed by the software Grasshopper, and its corresponding aliquot points of printing trajectory (determined by fabrication resolution of 1.25 mm), V, and H were written into fabrication G-codes (*.gcode) files using the software Grasshopper's plug-in GhPython Script. The obtained fabrication files can be recognized by the available 3D printer (Regenovo Bio-Architect® WS).

In the fabrication workflow **(Extended Data Fig. 6)**, first, the 3D printer was initialized

by its control software (3D Bio-Architect®). Second, after ink preparation, the gradient pore samples were manufactured by running customized fabrication G-code files through the control software (3D Bio-Architect®).

FDA-3D printing

To demonstrate the advantages of the FDA-3DP strategy in creating gradient pore structures, we designed and manufactured various gradient structures. These samples were manufactured from H-PCL ink using the extrusion 3D printer (Regenovo Bio-Architect® WS) with a heating temperature of 110 °C, a nozzle inner diameter of 400 μm, and an extrusion pressure of 500 kPa (see detailed printing parameters in **Supplementary Table 2**). The important 3D printing processes were recorded using a digital camera (Sony α7 II, Japan), including the coiling effect from the traditional-3DP strategy (**Supplementary Video 2**), the general deposition state from the FDA-3DP strategy (**Supplementary Video 3**), and the FDA-3D printing process of the horizontal gradient pore structure (**Supplementary Video 4**).

Coaxial printing

For coaxial printing, we fabricated the vascular sample and the pressure sensor using a coaxial nozzle with an inner needle of 17G and an outer needle of 22G. For the vascular sample (**Fig. 4c**), the core and shell materials were F127 and GelMA, respectively. The printed sample was UV cross-linked for 30 seconds, followed by placing them in deionized water to remove the F127. The obtained sample was immersed in deionized water for 3 hours and perfused using a syringe to remove F127. Finally, the perfusion experiment of the vascular scaffold was performed using a mixture of red dye and deionized water as a medium, and recorded using a digital camera (Sony α7 II, Japan) (**see Supplementary Video 8**).

For the pressure sensor (**Fig. 4d**), the core and shell materials were F127 and PDMS, respectively. For PDMS curing, the printed sample was placed in an incubator and heated at 60 °C for 6 hours. The obtained sample was immersed in deionized water for 3 hours and perfused using a syringe to remove F127. Then, the liquid metal EGaIn was filled into the cavity of the coaxial tube, and silver wires were placed at both ends of the tube. Finally, the sensor was sealed with PDMS and cured by heating again.

4D printing

To demonstrate the potential application of our proposed strategy in 4D printing (**Fig. 4e**), we designed an octopus-mimicking structure with eight 15 mm-long tentacles and prepared it using

pure alginate ink. The obtained alginate sample was cross-linked using a 1.0 M calcium ion solution (Ca^{2+}) for 30 seconds. As the solvent evaporation at room temperature (25 °C), eight tentacles of the sample gradually bent downward, and eventually supported the entire sample after about 1 hour. Their deformation was recorded using a digital camera (Sony α7 II, Japan) (**Supplementary Video 9**).

Filament cross-section quantification

Fixed-diameter filament samples were cut using a knife, and filament cross sections were photographed using a light microscope (HiROX MXB-5040RZ, Japan). We thus acquired the area S and aspect ratio AR of the cross sections using the software ImageJ (Fiji Is Just ImageJ, https://imagej.net/software/fiji/). The ideal diameter D was derived from the equation $D = (4S/\pi)^{0.5}$. The filament diameter obtained by this method was called the imaging result, shown in **Extended Data Fig. 3b**.

Fabrication resolution

We divided a 40 mm-long line segment into 4, 8, 16, 32, and 64 equal parts, respectively (i.e., fabrication resolution = 10, 5, 2.5, 1.25, and 0.625 mm, respectively). All 40 mm-long trajectories were given a V gradient of 2.1-13.1 mm/s (i.e., D = 0.3472-1.7358 mm based on equation (1): $D = (4Q/V\pi)^{0.5}$) and its corresponding H ($H \approx 0.8 \times D$) (**Extended Data Fig. 3f** and **Supplementary Figure 6**). The trajectory distance as a function of the ideal filament diameter is $D = 0.139 \times L + 0.347$ (red line, **Extended Data Fig. 3e**), where L is the trajectory distance from the printing position to the starting point. The 40 mm-long filaments printed via FDA-3DP strategy were scanned at 20 μm resolution using micro-computed tomography (μ-CT) equipment (SCANCO, Switzerland). Then, the obtained μ-CT images were treated with the tools CTAn and DataViewer from the SkyScan 1176 software package for gray segmentation and image rotation, thereby obtaining a series of filament cross-section images. Further, all cross-sectional images were batch-processed using the software ImageJ to obtain the cross-sectional area S, and the ideal diameter D was derived from the equation $D = (4S/\pi)^{0.5}$.

Pore size quantification

To quantitatively evaluate the gradient pores of printed samples, we scanned the samples at 12-20 μm resolution using μ-CT equipment (SCANCO, Switzerland). First, the obtained μ-CT images were treated with the tools CTAn and DataViewer from the SkyScan 1176 software package for gray segmentation, region of interest extraction, and x-y-z axis rotation. Note that

grayscale segmentation enables the cancellation of background noise and extraction of the pore structure within the sample. Then, the above obtained *x*-*y* plane images were analyzed using the BoneJ plugin's command 'thickness' in the software ImageJ, obtaining a series of *x*-*y* plane images. These *x*-*y* plane images were used to create the 3D model of the pore size map of the printed sample in ImageJ using the command '3D Viewer', as shown in **Figs. 3-4** and **Extended Data Fig. 9**. In addition, to further demonstrate the pore size distribution, these *x*-*y* plane images of the pore size maps were imported into software Adobe Premiere Pro CC (Adobe, USA) for generating videos showing the pore size variation in the *z*-axis direction (**Supplementary Videos 1**, **5**, and **6**).

μ-CT-based 3D reconstruction

The μ-CT images of all 3D printed samples were obtained by μ-CT equipment (SCANCO, Switzerland), and handled with tools CTAn for gray segmentation and region of interest selection. Then, the handled images were rotated to a horizontal-vertical orientation. Finally, 3D models were generated via the tool CTAn using the command 'Create 3D-model'.

Mechanical compression test of V-shaped metastructures

Metastructure samples with no, small, medium, and large gradients were subjected to uniaxial compression of 45% strain with a moving speed of 1 mm/s at room temperature (25 °C) using a universal mechanical machine with a pressure sensor of 500 kg (Dongguan Zhiqu company, China). The compression process was recorded using a digital camera (Sony α7 II, Japan) (**Extended Data Fig. 10** and **Supplementary Video 7**).

Pressure sensor test

Resistance measurements of the pressure sensor were performed using a digital multimeter (Keithley 2000, USA) in five zones (A to E, see **Fig. 4d**) through an 800 g weight (Suce company, China). The pressure on the sensor can be obtained as $F = mg$, where m is the mass of the weight, and g is the acceleration of gravity (9.78 m/s^2). For measurement accuracy, we printed two pressure sensors in parallel, then placed a thin plate above them at the interest zone, and finally placed the weights on the plate. Notably, only the resistance of the sensor at one position was measured for each experiment. Each measurement was conducted at an interval of ~5 seconds to make the LMs flow back to the initial position.

Flow rate measurement

The ink flow rate Q was measured by weighing ink extruded from the nozzle at a certain time ($Q = m/(\rho \times t)$), where m is the weight of the extrusion ink, ρ is the ink density, and t is the extrusion time. The flow rate Q obtained by this method was called the weighing result, as **shown in Extended Data Fig. 3a-b**.

CFD simulation of ink flow

The commercially available software COMSOL Multiphysics 6.0 (Dassault Systèmes, USA) was used to simulate the fluid flow of extruded ink through the nozzle at different printing conditions. The top and bottom of the nozzle domain were defined as the inlet and outlet, respectively. The remaining walls were set to be smooth and slip-free. The reference temperature was set to room temperature (25 °C). L-PCL (dynamic viscosity, 39 Pa s; density, 1303.5 kg/m^3) and H-PCL (dynamic viscosity, 318 Pa s; density, 1216.8 kg/m^3) were used as printing inks, and the inks were considered incompressible, continuous, and isotropic in the CFD simulation. The flow rate Q obtained by this method was called the CFD result, **shown in Extended Data Fig. 3a-b**.

Statistical analysis

The commercially available software OriginPro 2022 (OriginLab Corporation, USA) was used to analyze the data in this work. All data were reported as means ± standard error (means ± s.d.). Data were analyzed using one-way ANOVA and Tukey's test. When $^*P < 0.05$, $^{**}P < 0.01$, and $^{***}P < 0.001$, the differences in statistical analysis were accepted as significant. NS indicates no significant difference.

Supplementary Notes

Supplementary Note 1

Printing height *H* vs. ideal filament diameter *D* for keeping general deposition state

In the filament deposition state map, the general state was marked as solid triangles (**Extended Data Fig. 3c**), giving a fitting function ($H = 1.744\times(V)^{-0.5}$). Based on volume conservation, we obtained equation (1): $D = (4Q/V\pi)^{0.5}$. By combining the above two equations, the relation between H ($H = h$, only for the first layer) and D can be obtained ($H = 1.744\times(4Q/\pi)^{-0.5}/D$). After determining the working conditions (ink rheology of L-PCL, nozzle internal diameter of 400 μm, and extrusion air pressure of 400 kPa), the ink flow rate Q = 3.75 mm^3/s can be calculated by the weighing method (see Flow rate measurement in Materials and Methods). Then, the flow rate Q = 3.75 mm^3/s was substituted into the function $H = 1.744\times(4Q/\pi)^{-0.5}/D$, and the result suggests that H is approximately 0.8 times D ($H \approx 0.8\times D$).

Supplementary Note 2

Fabrication resolution vs. fabrication G-codes vs. its file size

The commercially available software Rhino and its tool Grasshopper were used to plot and plan the printing trajectory in the FDA-3DP strategy. Using this software, the printing trajectory (2D lines in the *x*-*z* or y-*z* plane) was equally segmented according to the fabrication resolution of 1.25 mm using the Grasshopper command "divide". The obtained equal points with *x*-*y*-*z* coordinates (*z* coordinate value is *H*) and their corresponding *V* were written as G-codes after adding the code start (initialization) and end commands (Supplementary Figure 7). Notably, the fabrication resolution determines the number of aliquots, and then affects the file size of the G-codes, as shown in **Extended Data Fig. 3e-f**. In this work, the fabrication resolutions of 10, 5, 2.5, 1.25, and 0.625 mm correspond to the divided numbers of 5, 9, 17, 33, and 65, respectively (**Supplementary Figure 6**).

Supplementary Note 3

Design-to-manufacturing workflow for the FDA-3DP strategy

The traditional-3DP strategy uses automated slicing tools (e.g., Cura, Simplify3D, and Slic3r) to obtain fabrication G-codes with the constant *V* and *H* within layers, and the printed samples have uniform pore structures. In this study, to implement the FDA-3DP strategy, first, we selected a conventional extrusion 3D printer (Regenovo Bio-Architect® WS) as a 3D builder. After determining the ink, the extrusion flow rate Q was obtained based on a weighing experiment or CFD simulation, resulting in a theoretical function of *V* versus *D* (see equation (1): $D = (4Q/V\pi)^{0.5}$). Then, we used the parametric tool Grasshopper to design the gradient pore

structure model, and obtained its corresponding V, H, and printing trajectory (moving point data). The above parameters were written into G-code files using the tool GhPython in Grasshopper based on the operation rules of the available 3D printer. Finally, the gradient pore matter can be manufactured by calling the customized G-codes using the 3D printer's control software (3D Bio-Architect®). Overall, we have built the design-to-manufacturing workflow for the new strategy, and its parametric design provides a one-click modification to create various pore gradients (**Extended Data Figs. 5-6**).

Supplementary Note 4

Filament cross-section vs. printing velocity *V*

The viscoelastic ink deposited by 3D printing is fluid and the filament cross-section is nearly oblong, as shown in **Extended Data Fig. 2a-m**. The relationship of V and AR are fitted ($AR = 2.457\times V^{-0.297}$), as shown in **Extended Data Fig. 2n**. According to the definition of AR, we can get $AR = l_w/l_h$ and $S = l_w/l_h - l_h^2\,(1-\pi/4)$ (**Extended Data Fig. 2o**). Based on equation (1), we can get $S = Q\times V^{-1}$. After determining the printing conditions (nozzle shape, nozzle inner diameter, extrusion pressure, and viscoelasticity ink), the ink flow $Q = 1.646$ mm^3/s can be obtained from the CFD simulation model. In addition, V for a series of movement points on the printing trajectory can be determined based on the gradient pores. Finally, based on the above four functions ($AR = 2.457\times V^{-0.297}$, $AR = l_w/l_h$, $S = l_w/l_h - l_h^2\,(1-\pi/4)$, and $S = Q\times V^{-1}$), the width l_w and height l_h at different V can be obtained.

References

1. Loessner, D.*, et al.* Functionalization, preparation and use of cell-laden gelatin methacryloyl–based hydrogels as modular tissue culture platforms. *Nat. Protoc.* **11**, 727-746 (2016).
2. Di Luca, A.*, et al.* Toward mimicking the bone structure: design of novel hierarchical scaffolds with a tailored radial porosity gradient. *Biofabrication* **8**, 045007 (2016).
3. Diaz-Gomez, L., Kontoyiannis P. D., Melchiorri A. J. & Mikos A. G. Three-dimensional printing of tissue engineering scaffolds with horizontal pore and composition gradients. *Tissue Eng. Part C-Methods* **25**, 411-420 (2019).
4. Qu, H.*, et al.* Fractal Design Boosts Extrusion-Based 3D Printing of Bone-Mimicking Radial-Gradient Scaffolds. *Research* **2021**, 9892689 (2021).
5. Xie, C.*, et al.* Structure-induced cell growth by 3D printing of heterogeneous scaffolds with ultrafine fibers. *Mater. Des.* **181**, 108092 (2019).
6. Shigueoka, M. O. & Volpato N. Expanding manufacturing strategies to advance in porous media planning with material extrusion additive manufacturing. *Addit. Manuf.* **38**, 101760 (2021).
7. Bittner, S. M.*, et al.* Fabrication and mechanical characterization of 3D printed vertical uniform and gradient scaffolds for bone and osteochondral tissue engineering. *Acta Biomater.* **90**, 37-48 (2019).
8. Diloksumpan, P.*, et al.* Orthotopic Bone Regeneration within 3D Printed Bioceramic Scaffolds with Region-Dependent Porosity Gradients in an Equine Model. *Adv. Healthc. Mater.* **9**, 1901807 (2020).
9. Grigolato, L., Rosso S., Meneghello R., Concheri G. & Savio G. Design and manufacturing of graded density components by material extrusion technologies. *Addit. Manuf.* **57**, 102950 (2022).
10. Moetazedian, A., Budisuharto A. S., Silberschmidt V. V. & Gleadall A. CONVEX (CONtinuously Varied EXtrusion): A new scale of design for additive manufacturing. *Addit. Manuf.* **37**, 101576 (2021).
11. Yuk, H. & Zhao X. A New 3D Printing Strategy by Harnessing Deformation, Instability, and Fracture of Viscoelastic Inks. *Adv. Mater.* **30**, 1704028 (2018).
12. Charbonnier, B.*, et al.* Custom-made macroporous bioceramic implants based on triply-periodic minimal surfaces for bone defects in load-bearing sites. *Acta Biomater.* **109**, 254-266 (2020).
13. Sun, Y.*, et al.* 3D-bioprinting ready-to-implant anisotropic menisci recapitulate healthy meniscus phenotype and prevent secondary joint degeneration. *Theranostics* **11**, 5160-5173 (2021).
14. Bahcecioglu, G., Hasirci N., Bilgen B. & Hasirci V. A 3D printed PCL/hydrogel construct with zone-specific biochemical composition mimicking that of the meniscus. *Biofabrication* **11**, 025002 (2019).
15. Zhang, Z.-Z.*, et al.* Orchestrated biomechanical, structural, and biochemical stimuli for engineering anisotropic meniscus. *Sci. Transl. Med.* **11**, eaao0750 (2019).
16. Bahcecioglu, G., Bilgen B., Hasirci N. & Hasirci V. Anatomical meniscus construct with zone specific biochemical composition and structural organization. *Biomaterials* **218**, 119361 (2019).
17. Li, Z.*, et al.* Biomechanically, structurally and functionally meticulously tailored polycaprolactone/silk fibroin scaffold for meniscus regeneration. *Theranostics* **10**, 5090-5106 (2020).
18. Guo, W.*, et al.* 3D-printed cell-free PCL–MECM scaffold with biomimetic micro-structure and micro-environment to enhance in situ meniscus regeneration. *Bioact. Mater.* **6**, 3620-3633 (2021).

Supplementary Figures

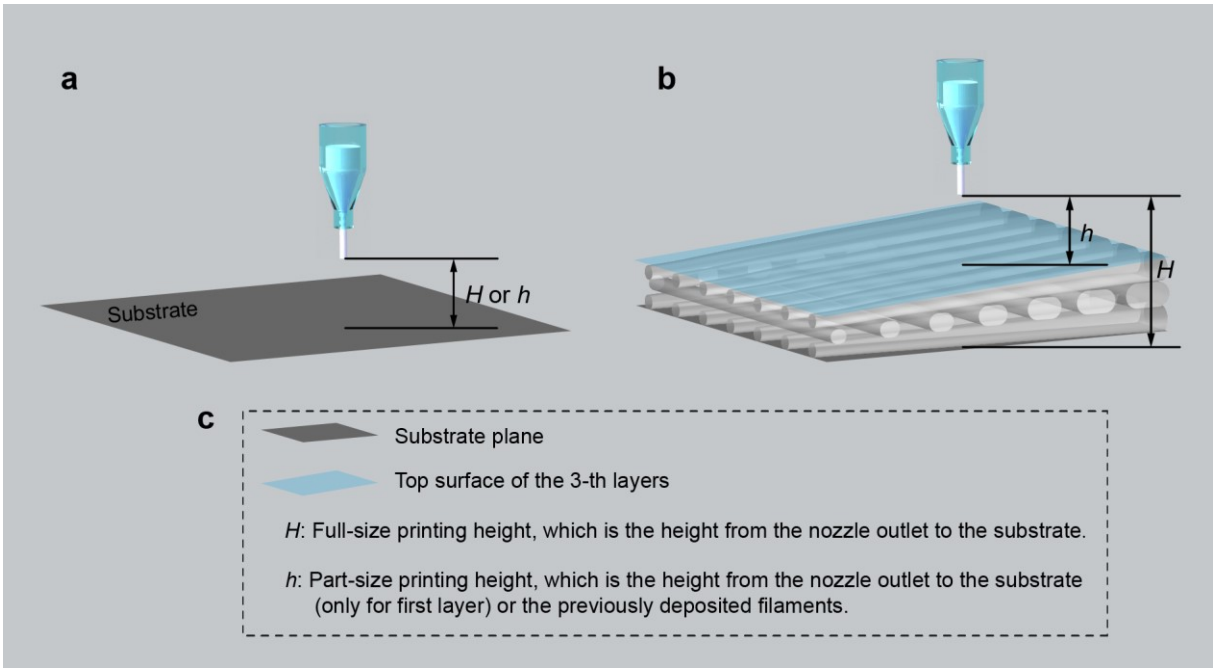

Supplementary Figure 1 | Definition of *H* and *h*. **a**, Schematic diagram of *H* and *h* in the only first layer condition. **b**, Schematic diagram of *H* and *h* in the multiple layer condition. **c**, Annotations for Supplementary Figure 1**a** and **b**. *H* is the height from the nozzle outlet to the substrate. *h* is the height from the nozzle outlet to the substrate (only for the first layer) or the previously deposited filaments.

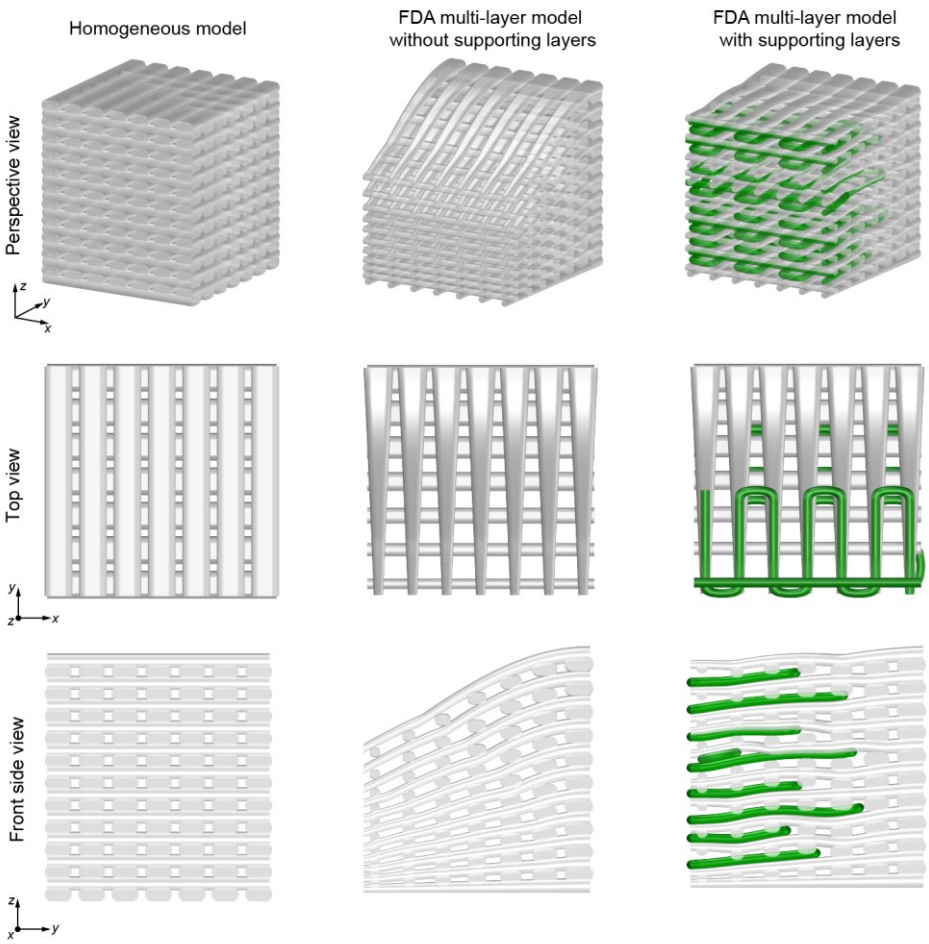

Supplementary Figure 2 | Details of the homogeneous model (left) and horizontal gradient pore models without (middle) and with (right) supporting layers. The traditional-3DP strategy is limited by the fixed D and the pore size is the same everywhere (left). In our proposed strategy, if it is not supported (middle), the horizontal gradient model has a collapse in the large pore region. Therefore, we added supporting layers with a constant minimum D_{min} (right, green filament model).

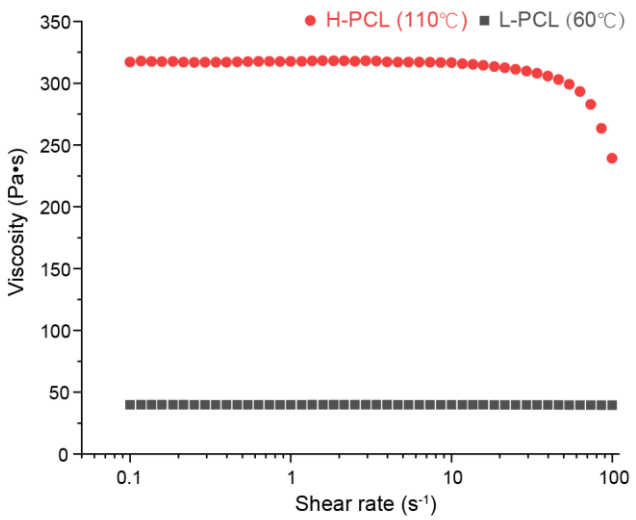

Supplementary Figure 3 | Rheology of H-PCL and L-PCL at 110 °C and 60 °C, respectively.

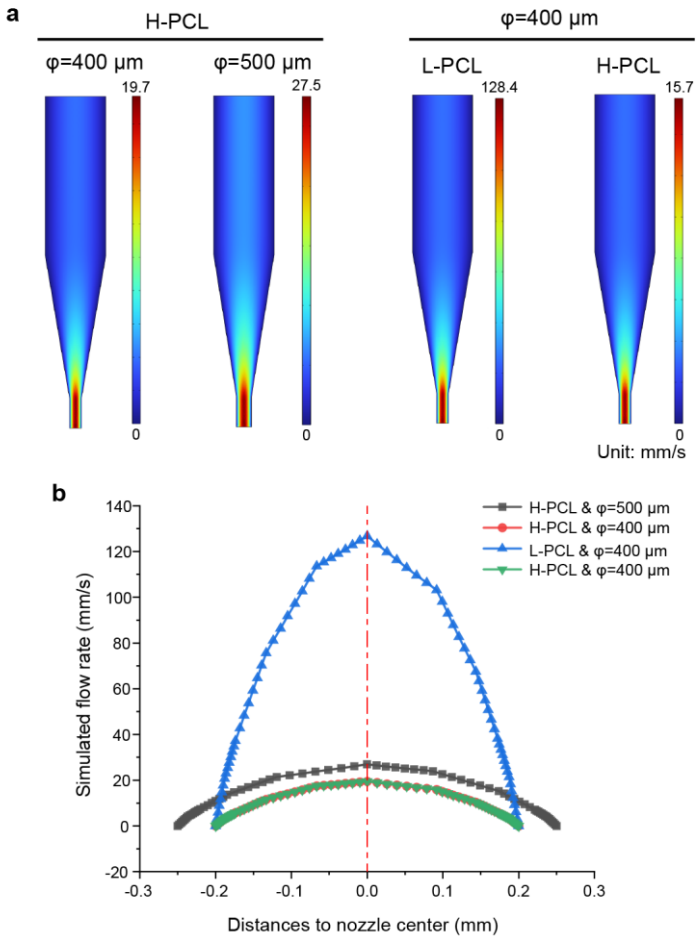

Supplementary Figure 4 | CFD simulation. **a**, Flow velocity field cloud maps at four working conditions, including the H-PCL and nozzle inner diameter (φ = 500 μm) group, the H-PCL and nozzle inner diameter (φ = 400 μm) group, the L-PCL and nozzle inner diameter (φ = 400 μm) group, and the L-PCL and nozzle inner diameter (φ = 400 μm) group. **b**, Quantification of flow velocity at the nozzle outlet.

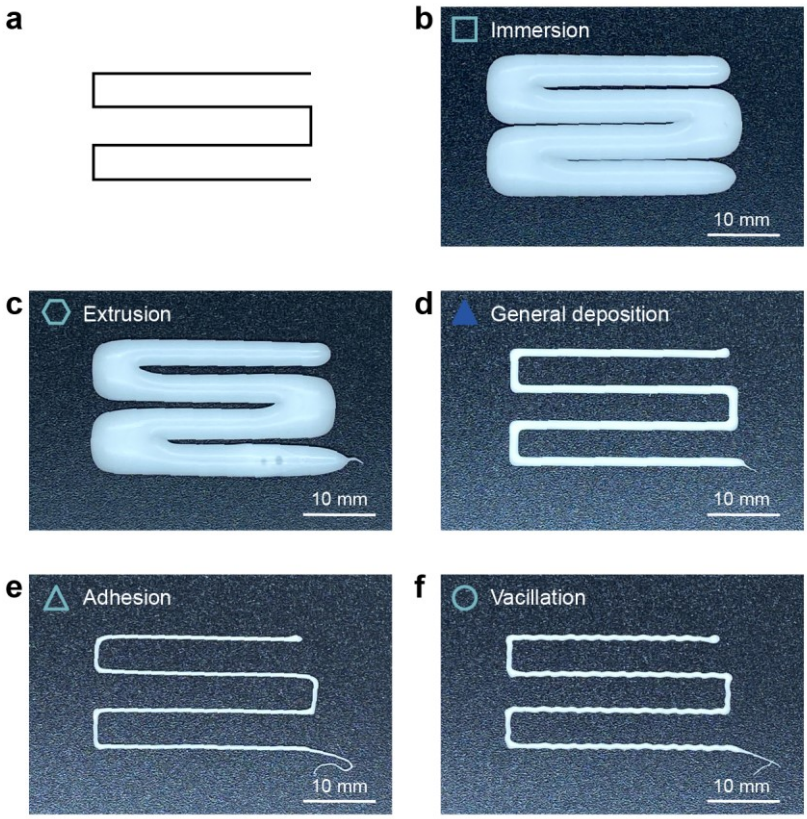

Supplementary Figure 5 | Printing trajectory and top views of printed filaments with five deposition states. **a**, Printing trajectory. **b-f**, 3D Printed single filament samples with different *V* and *H*, showing five deposition states. The filament deposition states include immersion, extrusion, general deposition, adhesion, and vacillation.

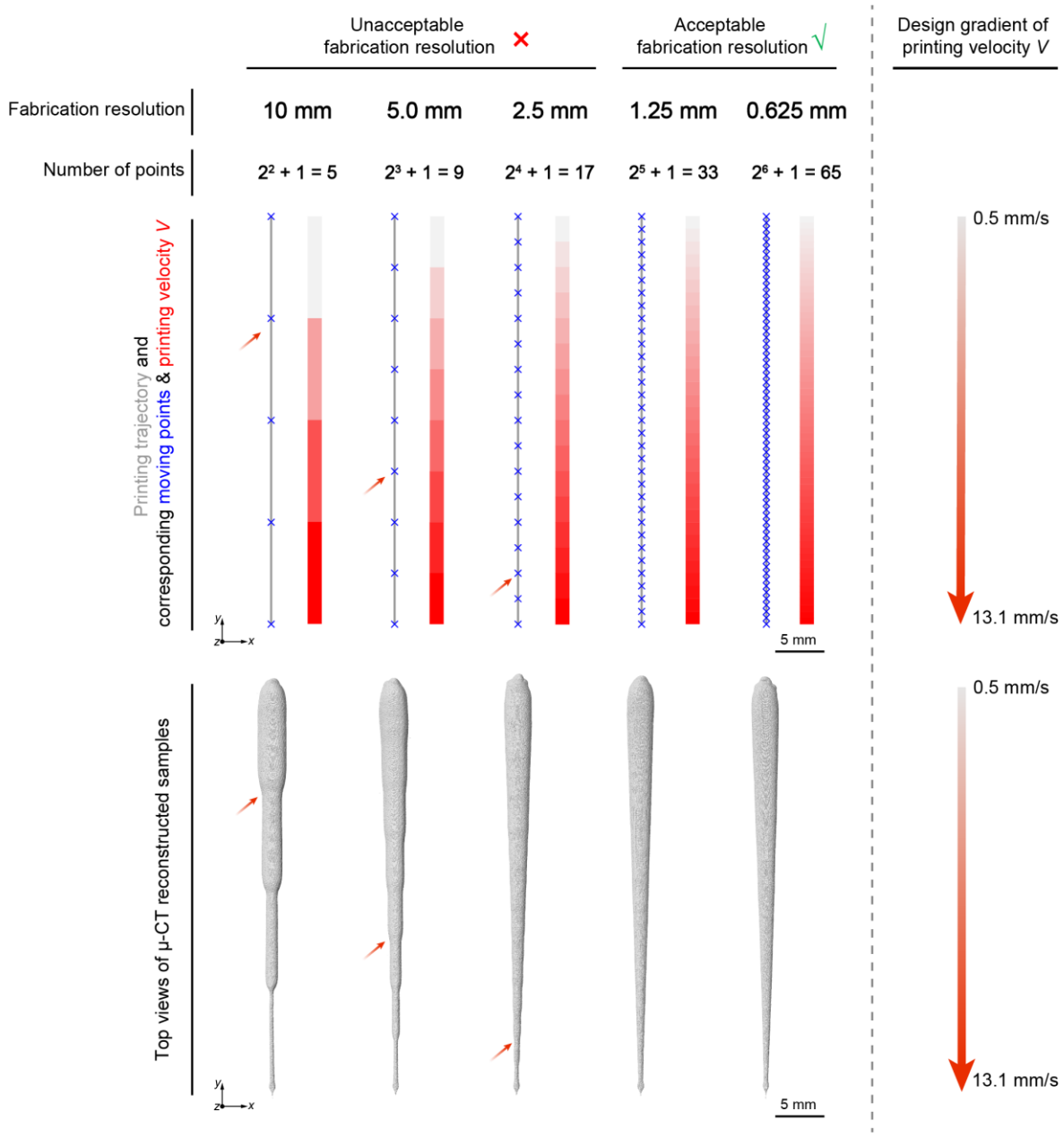

Supplementary Figure 6 | Printing trajectory, number of moving points, printing velocity, and top views of the μ-CT reconstructed 40 mm-long FDA samples with different fabrication resolution (10, 5.0, 2.5, 1.25, and 0.625 mm). In this figure, the gray line is the 40 mm-long printing trajectory; the blue cross is the movement points; the red rainbow chart is the design gradient of the printing velocity V; and the oblique red arrows show the step phenomenon. As the fabrication resolution increases, the tendency of the filament width l_w to vary uniformly increases significantly, and the step phenomenon (oblique red arrow) gradually disappears.

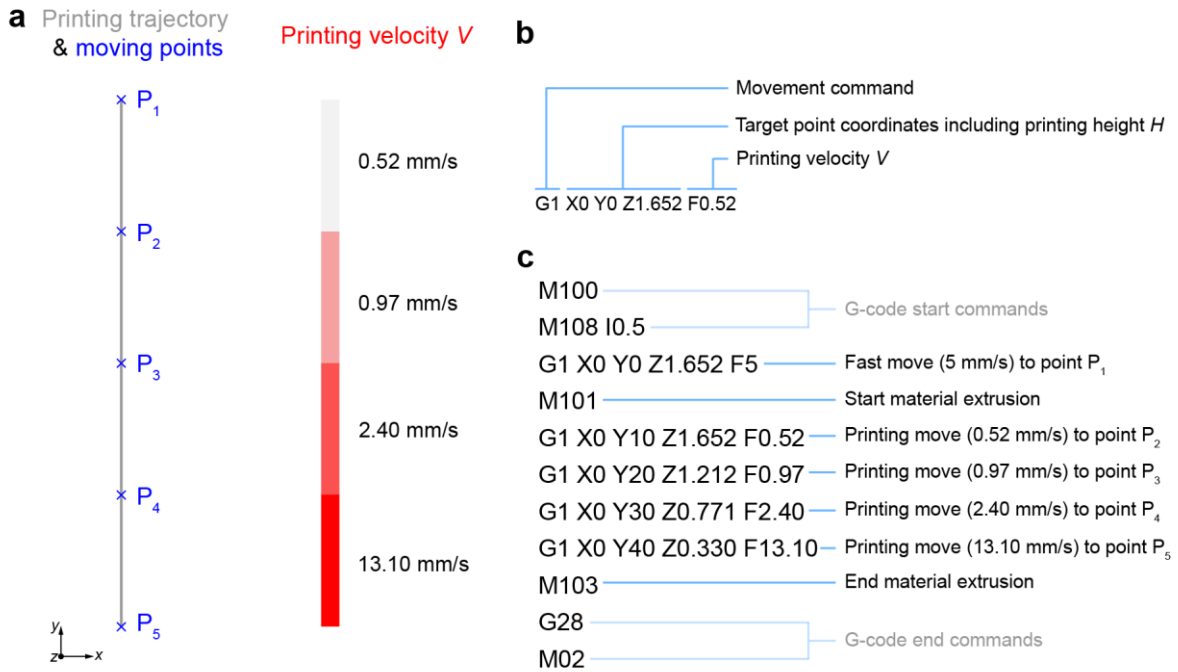

Supplementary Figure 7 | Printing trajectory, moving points, printing velocity (a), meaning (b)-(c) of fabrication G-codes of a 40 mm-long FDA filament. The fabrication G-codes consist of a sequence of 3D point coordinates (from P_1 to P_5) and their matching printing velocity V (from 0.52 to 13.10 mm/s) and height H (from 1.652 to 0.330 mm).

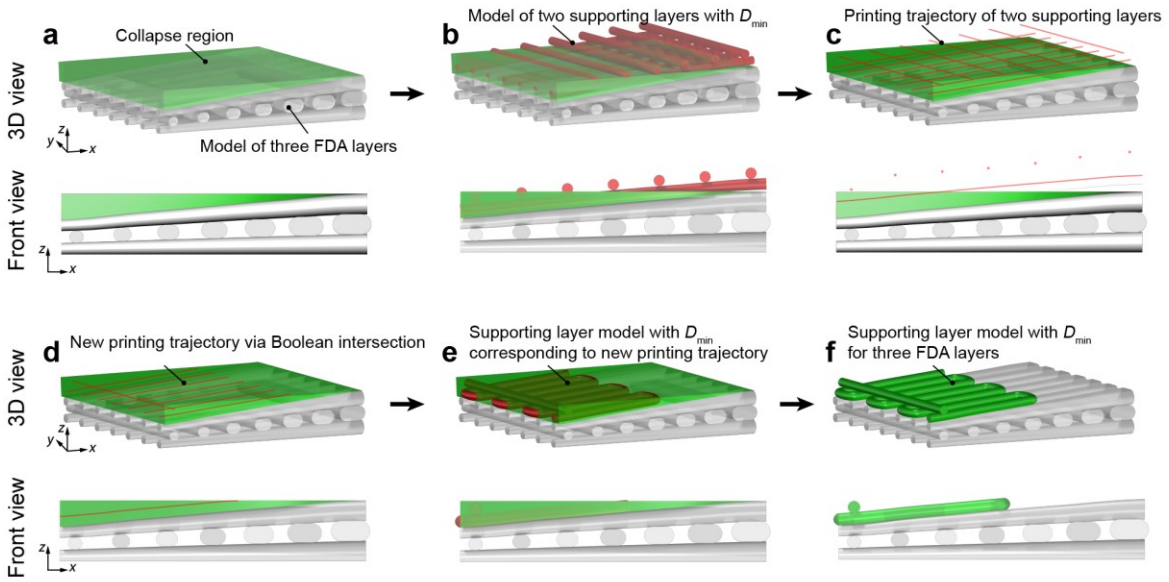

Supplementary Figure 8 | Steps of the thickness compensation algorithm for obtaining the printing trajectory and the 3D model of the supporting layers using Boolean intersection operations. The top and bottom sub-figures are the 3D view and the front view, respectively. **a**, Collapse region (green) for the three FDA layer model (grey). **b**, Model of two supporting layers with D_{min} (red) are positioned on top of the three FDA layer model (grey). **c**, Printing trajectory corresponding to two supporting layers. **d**, Result of the new printing trajectory obtained by Boolean intersection between the collapsed region and the printing trajectory of two supporting layers. **e**, New supporting layer model with fixed D_{min} by pipe operation. **f**, Result of supporting layer model for the three FDA layers.

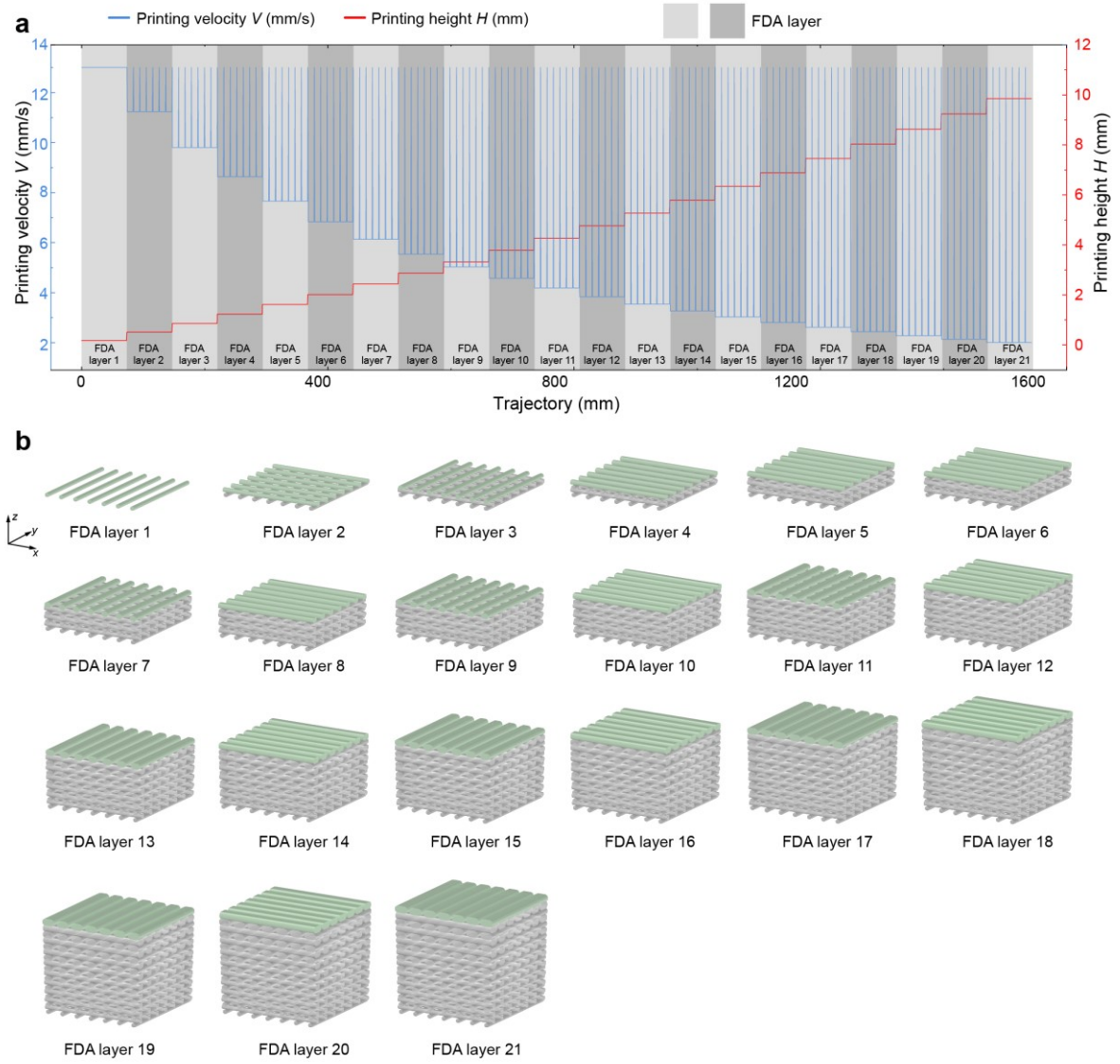

Supplementary Figure 9 | Phase diagram of printing parameters and filament stacking models of axial gradient model. a, Details of V and H. During the printing process, V and H gradually increase from bottom to top between layers. However, they remain constant within the layer. **b**, A series of axial gradient pore models with variable-D FDA layers. The final model was constructed by stacking 21-layer FDA filaments.

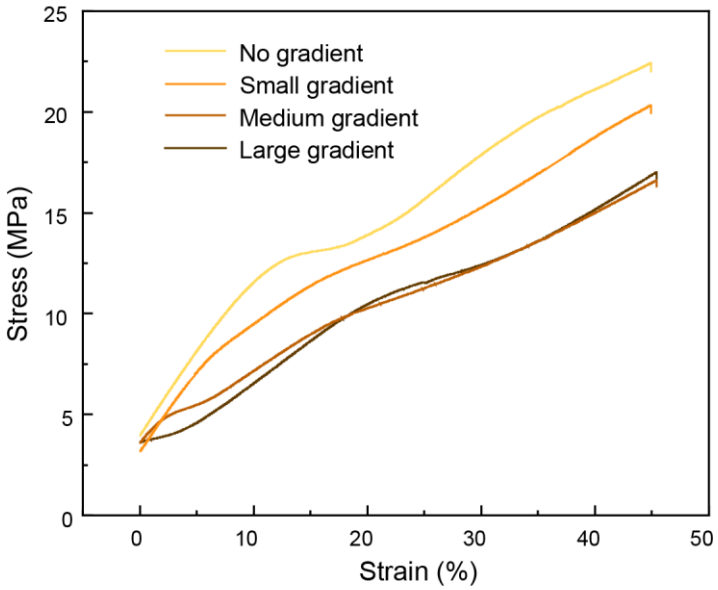

Supplementary Figure 10 | Compression test of four V-shaped metastructures.

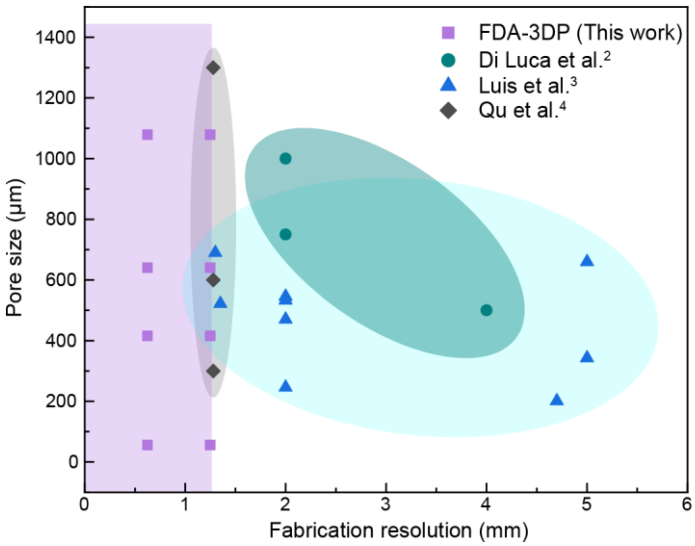

Supplementary Figure 11 | Comparison of fabrication resolution and pore size between FDA-3DP strategy and reported methods for extrusion 3D printed radial gradient pore structures. Our proposed proposed in this work has high fabrication resolution (≤1.25 mm) and a wide range of pore diameter sizes (56-1128 μm). Di Luca et al.[2] and Luis et al.[3] divided the target model into different areas along the radial direction and filled them with variable diameters and spacing filaments. Qu et al.[4] proposed a fractal iterative method to design filling patterns and constructed radial gradient pores.

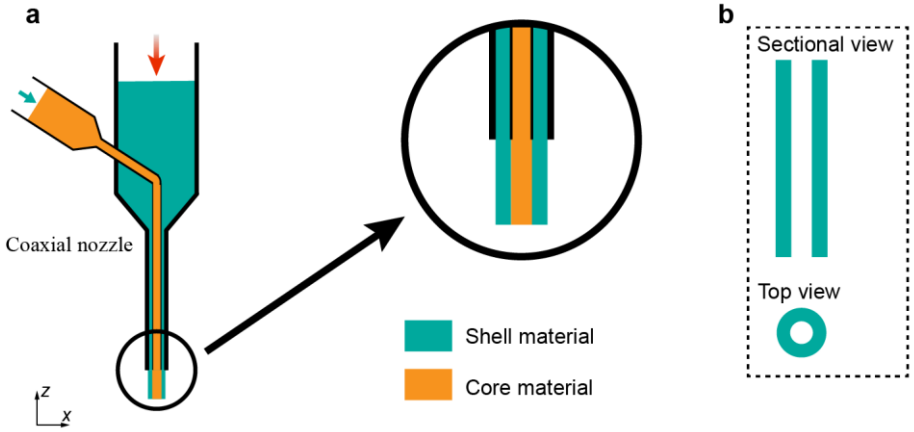

Supplementary Figure 12 | Schematic diagram of coaxial nozzle. For preparing the vascular scaffold, GelMA and F127 are used as the shell and core materials, respectively (**Fig. 4c**); in the pressure sensor, PDMS and liquid metal (EGaIn) are used as the shell and core materials, respectively (**Fig. 4d**).

Supplementary Tables

Supplementary Table 1 | A comparison between the FDA-3DP strategy and the reported DIW 3D printing methods for creating gradient pore structures, focusing on gradient dimension, gradient resolution, and shape fidelity. A check mark (✓) denotes feasibility or compatibility, while a wrong mark (✗) denotes infeasibility or unattainability. A hyphen mark (-) indicates not mentioned in the literature.

Changing parameters	Gradient dimension[1]				Gradient resolution[2]	Shape fidelity[3]		Ref.
	1D			2D & 3D	Resolution level	Fidelity level	No collapse	
	Horizontal	Axial	Radial					
Diameter/spacing/angle within layers	✓	✗	✗	✗	Low	Low	✗	2,3,5,6
Diameter/spacing between layers	✗	✓	✗	✗	Medium	Medium	✓	7,8
Diameter/spacing in radial regions	✗	✗	✓	✗	Medium	Low	✗	2-4
Width of oblong filaments	✓	✓	✓	2D ✓ 3D ✗	High	Low	✗	9-11
Diameter & selectively adding support layers	✓	✓	✓	✓	High	High	✓	**This work**

[1] Gradient dimension includes 1D, 2D, and 3D. 1D represents one direction of the xyz coordinate axis.
[2] Gradient resolution indicates the ability to create gradient pores.
[3] Shape fidelity is the difference between the designed model and the fabricated sample.

Supplementary Table 2 | Parameters of printed samples shown in this work. Coaxial printing (Fig. 4c-d) and 4D printing (Fig. 4e) were performed at room temperature (25 °C), and the remaining 3D printing (gray background area) was done at 110 °C and extrusion pressure of 500 kPa using H-PCL material.

Location	Gradient	Model size (mm)	Fiber spacing (mm)	Printing velocity *V* (mm/s)	Nozzle height *H* (mm)	Pore size *D* (μm)
Fig. 1b	No	10×10×10	1.5	3	0.30	448
Fig. 1d	Horizontal	10×10×10	1.5	2.1-13.1	0.33-0.18	0-1128
Fig. 3a	Penetration	20×10×10	0.83	Min=5, Max=13	0.25, 0.18	0-640
	Centration					
	Cent. & Rot.					
Fig. 3b	No	10×10×10	0.82	5	0.25	210, 217
	Small	10×10×10	0.82	Min=5, Max=8	0.25, 0.22	215, 388
	Medium	10×10×10	0.82	Min=5, Max=11	0.25, 0.19	220, 486
	Large	10×10×10	0.82	Min=5, Max=14	0.25, 0.18	212, 514
Fig. 4a	Radial	φ10×15	1.5	2.1-13.1	0.33-0.18	0-1092
Fig. 4b	Radial	∠14.33°	Varying	2.1-13.1	0.33-0.18	377-943
Fig. 4c	Linear	Length 40	-	1.1-10	0.30-0.90	-
Fig. 4d	Linear	Length 25	-	0.75-2.9	0.5-1.30	-
Fig. 4e	Linear	Radius 15	-	1.1-10	0.30-0.90	-
ExFig. 3d	Linear	Length 20	-	Min=3, Max=8	0.30, 0.80	-
ExFig. 3e	Linear	Length 40	-	0.5-13.1	0.33-1.65	-
ExFig. 9	Axial	10×10×10	1.5	2.1-13.1	0.33-0.18	0-1176
	Point	10×10×10	1.5	2.1-13.1	0.33-0.18	0-1176
	Line	10×10×10	1.5	2.1-13.1	0.33-0.18	0-1176
	Surface	10×10×10	1.5	2.1-13.1	0.33-0.18	0-1176
	Body	10×10×10	1.5	2.1-13.1	0.33-0.18	0-1176

Supplementary Table 3 | A comparison for creating a bone-mimicking scaffold between the FDA-3DP strategy and the reported methods. A check mark (✓) denotes feasibility or compatibility, while a wrong mark (✗) denotes infeasibility or unattainability. Repetition of symbols indicates degree.

Strategies	CAD model	Printed sample	Radial gradient	Features	Ref.
Triply-periodic minimal surfaces (TPMS)	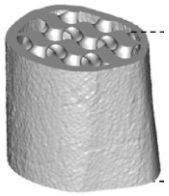	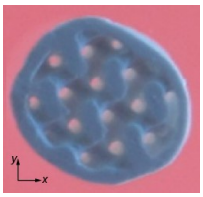	✗	Homogeneous pore and bionic cancellous-cortical bone	12
Conventional grid (0°/90°) via adjusting filament spacing between layers	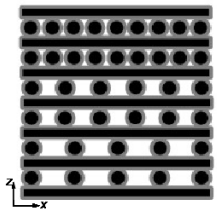	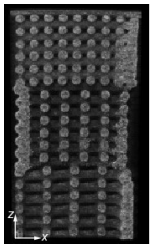	✗	Axial gradient	7
Conventional grid (0°/90°) via adjusting filament diameter in local regions	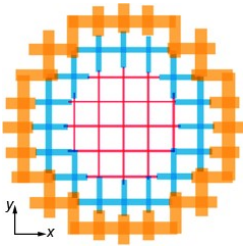	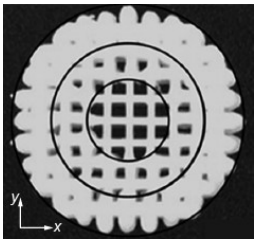	✓	Radial gradient, low gradient resolution, and height limitation	2,3
Fractal iterative pattern	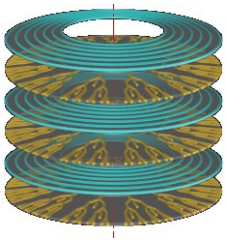		✓	Radial gradient, but low gradient resolution	4
FDA-3D printing strategy based on conventional grid (0°/90°)		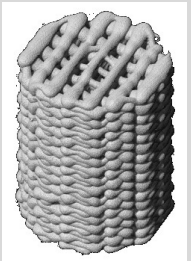	✓✓✓	Easy molding and highly tunable radial gradient	**This work**

Supplementary Table 4 | A comparison for creating a meniscus-mimicking scaffold between the FDA-3DP strategy and the reported methods. A check mark (✓) denotes feasibility or compatibility, while a wrong mark (✗) denotes infeasibility or unattainability. Repetition of symbols indicates degree.

Strategies	CAD model	Printed sample	Radial gradient	Features	Ref.
Conventional grid (0°/90°)			✗	No wedge cross section and no radial gradient	13
Conventional grid (0°/90°)	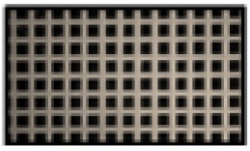	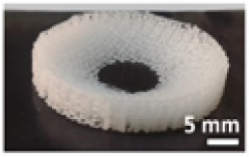	✗	No wedge cross section and no radial gradient	14
Radial and circular lines	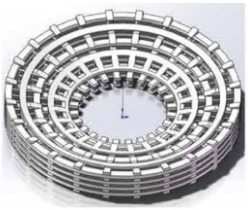	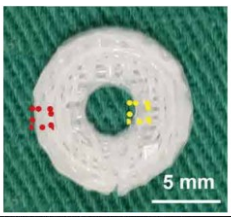	✓	Needs trimming and low tunable radial gradient	15
Grid (0°/90°) and Radial lines	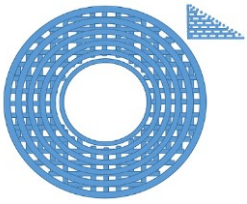	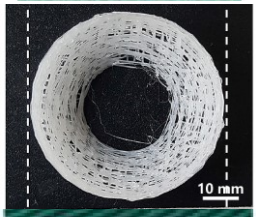	✓	Wedge tops difficult to fidelity and no radial gradient	16
Radial and circular lines			✓	Easy molding and low tunable radial gradient	17
Radial and circular lines	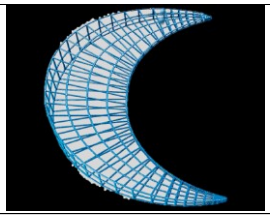	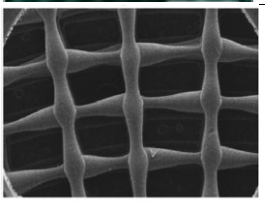	✓	Easy molding and low tunable radial gradient	18
Radial and circular lines via FDA-3D printing strategy	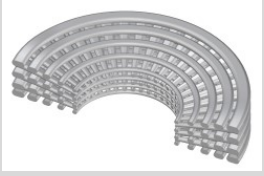	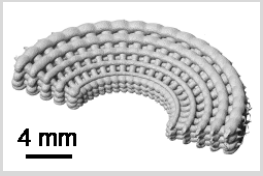	✓✓✓	Easy molding and highly tunable radial gradient	**This work**

Supplementary Videos

Supplementary Video 1 | Pore size maps of traditional- and FDA-3DP strategies. A horizontal gradient was chosen as an example to demonstrate the ability of the FDA-3DP strategy to create gradient pores. The video shows 2D images (*x*-*y* plane view) of printed samples and their pore size maps, and they appear gradually as the *z* height increases from bottom to top. The 2D images of printed samples were the μ-CT images, and their pore size maps were obtained by processing the μ-CT images using the software ImageJ. The samples obtained from the traditional- and FDA-3DP strategies have homogeneous and heterogeneous pore structures, respectively. The maximum pore size is 1128 μm.

Supplementary Video 2 | FDA-3D printing with constant printing height. A 20 mm-long printing trajectory is divided into two equal parts and set to two printing velocities (V = 3 and 8 mm/s), but they have a fixed printing height (H = 1.5 mm). During 3D printing, the first 10 mm-long trajectory shows an unacceptable rope coiling effect, and the last 10 mm-long trajectory presents an acceptable deposition state (see the constant H group in Extended Data Fig. 3d). The video is not accelerated or decelerated (1x).

Supplementary Video 3 | FDA-3D printing with variable printing height. A 20 mm-long printing trajectory is divided into two equal parts and set to two printing velocities (V = 3 and 8 mm/s) and corresponding variable printing height (H = 0.7 and 0.4 mm) based on the FDA-3DP strategy. During 3D printing, the whole 20 mm-long trajectory shows an acceptable and expected filament deposition state (see the variable H group in Extended Data Fig. 3d). The video is not accelerated or decelerated (1x).

Supplementary Video 4 | FDA-3D printing of horizontal gradient pore structure. The video shows the stacking process of 21 FDA layers and 8 supporting layers. The printing parameters in the video is from Fig. 2i. Here, the FDA layer filaments have variable D (depending on pore size gradient) and H; and the supporting layer filaments have a constant D_{min}. The video playback speed is fast forwarded four times (4x).

Supplementary Video 5 | Pore size maps of axial and radial gradient pore structures. The radial gradient includes point, line, surface, and body. The *x*-*y* intercept plane of the pore size map appears gradually as the *z* height increases from bottom to top. The result shows that the pore size of the axial sample gradually decreases from bottom to top; the pore size of the point-interfering sample is the largest in the center position, showing a regular radial gradient, and

gradually decreases from the center to the upper and lower positions; the pore size of line-interfering sample has a consistent radial gradient from the bottom to the top; the pore size of the surface-interfering sample is the largest at the location of the cylindrical surface; the pore size of the body-interfering sample is large in the middle position and small in the upper and lower positions. 2D images (*x*-*y* plane) of pore size maps were obtained by processing the μ-CT images using the software ImageJ. The maximum pore size is 1176 μm.

Supplementary Video 6 | Pore size maps of gradient structures with embedded HIT letters. The positions of HIT letters (abbreviations of Harbin Institute of Technology) include penetration, centration, and centration & rotation. Notably, in the penetration group (lift), the full HIT letters can be viewed in all *x*-*y* planes of the pore size map from bottom to top. In the centration group (middle), the full HIT letters can only be observed in the middle position, not in the upper and lower positions. In the centration & rotation group (right), only the partial part of the HIT letters can be visualized in the middle position, not in the upper and lower positions. 2D images (*x*-*y* plane) of pore size maps were obtained by processing the μ-CT images using the software ImageJ. The maximum pore size is 640 μm.

Supplementary Video 7 | Compression test of metastructures. Three metastructures with embedded V letter have small, medium, and large gradients. A homogeneous pore sample is used as a control group. The video playback speed is fast forwarded four times (4x). Scale bar is 5 mm.

Supplementary Video 8 | Penetration of vascular scaffold. The upper scaffold has tunable width l_w and uniform straightness, and the lower scaffold not only has a controllable width, but also can realize the controllable fluctuation. The perfusion medium is red dye water, and the silver-white materials inside the scaffold are bubbles before the red ink enters. The video is played at normal speed (1x). Scale bar is 10 mm.

Supplementary Video 9 | 4D printing. Octopus-mimicking alginate sample with eight tentacles was deposited on the substrate via the FDA-3DP strategy and then cross-linked using a 1.0 M calcium chloride solution (Ca^{2+}) for 30 seconds. The cross-linked alginate sample was left at room temperature (25 °C). As water evaporated, eight tentacles gradually bent downward, eventually supporting the entire sample after about 1 hour. The video playback speed is fast forwarded a hundred times (100x). Scale bar is 5 mm.